Premixed Flame Response to Unsteady Strain-Rate and Curvature

Habib N. Najm* and Peter S. Wyckoff

Sandia National Laboratories
P.O.Box 969, MS 9051
Livermore, CA 94551, USA
Tel/Fax: (510) 294-2054/1004
email: hnnajm@ca.sandia.gov

Word Length: Text: 3700, Figures: 1400, Tables: 550.

Total: 5650.

Presentation preference: Oral presentation.

Colloquium topic area preference: Laminar flames.

* Corresponding Author

Abstract

The interaction of a premixed stoichiometric methane-air flame with a counter-rotating vortex-pair is studied using a skeletal C_1 chemical description of the reaction process. The focus is on the modification to flame structure and dynamics due to unsteady strain-rate and curvature. The detailed description of flame structure and dynamics in response to unsteady flow is necessary to establish relevant extinction criteria in unsteady multi-dimensional flow, which, based on recent experimental evidence, may be significantly different from those of steady one-dimensional counterflow stagnation flames. Present results suggest that the increasing unsteady tangential strain-rate causes modification of flame structure that leads to reduced reaction rates of key chain-branching reactions which are active on the products side of the flame. This causes a reduction in the concentrations of active radicals, such as H, OH, and O, which are necessary for the breakdown of hydrocarbons on the reactants side of the flame.

Introduction

The detailed dynamical complexity of turbulent reacting flow is far beyond present computational modeling as well as experimental diagnostic capabilities. Therefore, it is useful to consider simpler flows that carry some of the generic features of turbulent flame-flow interaction. Both one-dimensional (1D) and two-dimensional (2D) flames have been studied in the literature to assess the influence of two key features of turbulent-flow-flame coupling, strain-rate and curvature, on the reaction process.

The bulk of existing data on premixed flame response to stretch is based on steady-state 1D opposed jet flame studies[1]. Flame response has been generally correlated with the Lewis number (Le) of the deficient reactant. Thus, the peak reaction rate is observed to decrease with increasing stretch rate for $Le > 1$ flames, leading to extinction. Whereas, for $Le < 1$, the reaction rate increases with stretch, and extinction occurs primarily due to short residence time as the flame penetrates the stagnation surface. Unity Le flames are found to extinguish similarly, but with no change in peak reaction rate with stretch until the flame reaches the stagnation surface.

Generally, opposed-jet stretched premixed flames have been studied more with regards to the response of integral quantities, such as overall "reaction rate", rather than that of individual reaction rates, or intermediate species concentrations. Recent work[2,3] regarding the role of particular intermediates and reactions in the extinction process has pointed out the key role of H atoms and specific chain-branching reactions in maintaining the chemical reaction process in the flame. In particular, Kee *et al.*[2] point out the high sensitivity of the maximum flame temperature near extinction to the reaction: $H+O_2 \Longleftrightarrow O+OH$, a key chain branching reaction limited by H atom availability.

The extension of these results to 2D unsteady vortical flame-flow interaction is not straightforward. The transient response of both intermediates and stable species, as well as temperature profiles, to strain-rate introduces significant changes to the simpler steady-state 1D opposed-jet picture. Curvature effects in 2D present an additional local dependence on flame geometry, absent in the 1D case. Previous modeling studies of flame-vortex interaction used simple single-step chemistry[4,5,6]. Some recent modeling work has begun to address the flame response in unsteady vortical 2D flow, using both reduced and detailed

chemical mechanisms[7,8,9]. However, there remain many unanswered questions regarding the extinction process in 2D unrestrained flow. Specifically, how relevant are the extinction strain-rates available from 1D steady flame studies in higher dimensional flow? What is the mechanism of extinction in the transiently stretched flame in 2D?

To this end, we study the stoichiometric methane-air flame interaction with a 2D counter-rotating vortex-pair, using a skeletal C_1 chemical description of the reaction process at the flame, with a focus on the modification to flame structure and dynamics due to unsteady strain-rate and curvature. Results suggest that the increasing unsteady tangential strain-rate leads to modification of the flame structure which affects those chain-branching reactions active on the products side of the flame, causing a reduction in the concentrations of active radicals, such as H, OH, and O, which are necessary for the breakdown of hydrocarbons on the reactants side of the flame.

Formulation

The governing equations are presented in their non-dimensional form in 2D. The assumptions of zero bulk viscosity[10], negligible body forces, and low Mach number[11] give the conservative continuity and momentum equations:

$$\frac{\partial \rho}{\partial t} + \nabla \cdot (\rho \mathbf{v}) = 0 \tag{1}$$

$$\frac{\partial(\rho u)}{\partial t} + \frac{\partial(\rho u^2)}{\partial x} + \frac{\partial(\rho uv)}{\partial y} = -\frac{\partial p}{\partial x} + \frac{1}{Re}\Phi_x \tag{2}$$

$$\frac{\partial(\rho v)}{\partial t} + \frac{\partial(\rho vu)}{\partial x} + \frac{\partial(\rho v^2)}{\partial y} = -\frac{\partial p}{\partial y} + \frac{1}{Re}\Phi_y \tag{3}$$

where ρ is the density, $\mathbf{v} = (u, v)$ is the velocity vector, p is the pressure, and Φ_x,Φ_y are the viscous dissipation terms.

We assume a detailed chemical reaction mechanism, involving N species, and M elementary reactions. The energy equation is developed allowing for variable transport properties, and a constant stagnation pressure p_o, *i.e.* an open domain. We neglect Soret and Dufour effects[12] and radiant heat transfer, and assume a perfect gas mixture, with individual species molecular weights, specific heats, and enthalpies of formation, using Fickian binary mass diffusion. Written in terms of temperature, the low Mach number energy equation is:

$$\frac{\partial T}{\partial t} = -\mathbf{v} \cdot \nabla T + \frac{1}{RePr}\frac{\nabla \cdot (\lambda \nabla T)}{\rho c_p} + \frac{1}{ReSc}\frac{\mathbf{Z} \cdot \nabla T}{c_p} + Da\frac{w_T}{\rho c_p} \tag{4}$$

with $\mathbf{Z} = \sum_{i=1}^{N} c_{p,i} D_{iN} \nabla Y_i$, and where $c_{p,i}$ is the specific heat of the i-th species at constant pressure, $c_p = \sum_{i=1}^{N} Y_i c_{p,i}$ is the corresponding mixture specific heat, T is the temperature, λ is the thermal conductivity, w_T is the chemical heat release source term, $w_T = -\sum_{i=1}^{N} h_i w_i$, $h_i = h_i^o + \int_{T^o}^{T} c_{p,i} dT$, and w_i is the production rate of species i.

The N-th species is assumed dominant such that the diffusion velocity of any other species i in the mixture is approximated by $\mathbf{V}_i = -D_{iN} \nabla Y_i / Y_i$, where D_{iN} is the binary mass diffusion coefficient of species i into the N-th species at the mixture local temperature and stagnation pressure, and Y_i is the mass fraction of species i. $\mathbf{V}_N$ is found from the identity $\sum_{i=1}^{N} Y_i \mathbf{V}_i = 0$. Further, for computational efficiency, mixture transport properties (μ,λ) are set to those of the N-th species at the local temperature.

The i-th species conservation equation, for $i = 1, \ldots, N-1$, is written as

$$\frac{\partial(\rho Y_i)}{\partial t} = -\nabla \cdot (\rho \mathbf{v} Y_i) + \frac{1}{ReSc}\nabla \cdot (\rho D_{iN} \nabla Y_i) + Da\, w_i, \tag{5}$$

and the mass fraction Y_N is found from the identity $\sum_{i=1}^{N} Y_i = 1$.

The perfect gas state equation is: $p_o = \rho T/\overline{W}$, where $\overline{W} = 1/\sum_{i=1}^{N}(Y_i/W_i)$, is the local effective molar mass of the mixture. The production rate for each species is given by the sum of contributions of elementary reactions[12], with Arrhenius rates $\mathcal{K}_k = A_k T^{b_k} e^{-E_k/RT}$, $k = 1 \ldots M$.

The above equations are solved using a second-order predictor-corrector finite difference projection method[6].

Results

We study the interaction of a premixed stoichiometric methane-air flame with a counter-rotating vortex pair in 2D, under atmospheric pressure conditions. The premixed reactants gas mixture composition is at ambient temperature 298K. The chemical mechanism is a skeletal C_1 reaction set, given in Table 1. This mechanism is that used in [13], with more recent rate coefficients from [14]. Flame profile data is shown in Fig. 1, in comparison with the GRImech1.2 C_1-C_2 data[14]. Generally, there is better quantitative agreement in the mole fractions of the major stable species, with qualitative agreement throughout. The burning speeds predicted by the present mechanism and GRImech1.2, using Chemkin[15,16] in 1D, are 38.8 and 39.1 cm/sec, respectively.

The 2D flow domain is a 0.8×0.5 cm^2 region, with periodic boundary conditions in the horizontal x-direction, and inflow-outflow boundary conditions in the y-direction. The initial condition is a superposition of the velocity (u,v) field due to a row of vortex pairs along x, and the (T,ρ,Y_i) fields in the y-direction from a 1D premixed flame solution based on the above mechanism using Chemkin. The Chemkin solution is relaxed on a 1D uniform grid prior to use in the 2D model. The vorticity field causes significant contortion of the flame profile, as shown in Fig. 2, leading to large variations in curvature and tangential stretch rate along the flame. Note the baroclinic vorticity dipole generated in the neighborhood of each of the original vortices, in agreement with the measurements of Mueller *et al.*[17]. The average flame thickness, and laminar burning (displacement) speed, defined in the appendix, are $\delta_f \approx 0.035$cm and $S_L = S_d^u \approx 35$cm/sec respectively. Then, with the convective length and velocity scales given by the vortex core size, $\delta_v \approx 0.25$cm, and the circumferential flow velocity $U_\theta \approx 20$m/sec, the flame and convective time scales are found to be $t_f = \delta_f/S_L = 1$ msec, and $t_v = \delta_v/U_\theta = 0.13$ msec respectively, and the corresponding Damköhler number is $Da = t_v/t_f = 0.13$. With $Da < 1$, the flow is faster than the flame, and it is expected that significant contortion of the flame will occur, as observed here, leading to a well-stirred condition at later time[18].

By defining the flame location for diagnostic purposes, as indicated in the appendix, we determine the flame normal, and evaluate the strain-rate and curvature along the flame length. Figure 3 shows the variation of tangential strain-rate τ_t and curvature κ for the

flame in Fig. 2, plotted versus flame length, with an origin at the flame intersection with the domain boundary, and extending to the vertical centerline. The curvature plot identifies clearly the location of curved flame cusp in Fig. 2, with large positive curvature. At the same location, there is considerable variation in τ_t from large positive stretch values on both sides of the cusp, to a large negative compressive strain-rate in the cusp region. The rest of the flame shows relatively minor rates of change of strain-rate, with a gradual decay to a low value with distance away from the centerline, to the left of the cusp, and with a broad peak value at the centerline. Tangential strain-rate at the centerline is $14 \times 10^3 \mathrm{s}^{-1}$. The normal strain-rate varies along the flame in an inverse fashion, with a large positive normal stretch at the cusp, and a broad compressive peak at the centerline. The total flame stretch[19] $K = \tau_t + S_d\kappa$ is largely dominated by the strain-rate, and hence varies along the flame as τ_t.

The above contortion and large stretch rates affect the flame significantly leading to local variation in the reaction rates. This is illustrated in Figs. 4 and 5, where the heat source term w_T, and the production rate of H, w_{H}, are shown plotted for the flame in Fig. 2. The w_{H} contours reveal the bi-layer structure of the flame. Net consumption of H occurs in the fuel consumption layer on the reactants side of the flame, where H is required by reactions (*e.g.* 11,14,16) that involve the breakdown of CH_4 through various intermediate hydrocarbons towards CO. The net production of H occurs in the oxidation layer on the products side of the flame, and involves reactions such as 3,9, and 2. This bi-layer picture pertains to the *net* production and consumption rates of H. Notably, Rxns. 13 and 17 involving the breakdown of CH_3 and HCO are H producers, while Rxn. 1 is a dominant H consumer, and a key chain branching step on the products side of the flame[2].

The variation of w_{H} in the curved cusp region is an interesting example of diffusional focusing and de-focusing effects related to flame curvature[1]. The production of H (Rxns. 13,3,17,9,2) involves precursors that are supplied by diffusion from the fuel-consumption layer. These precursors are focused into the oxidation layer due to the flame curvature, leading to enhanced fluxes and faster reaction rates. On the other hand, the consumption of H in the fuel consumption layer requires its diffusion from the oxidation layer, as well as thermal diffusion from the products, both of which are de-focused due to flame curvature. Thus, the H consumption rate is low in this region. This is reflected also in the consumption rate of CH_4, in the various elementary reaction rates, and in the overall burning process at

the flame, leading to a low w_T in this region, as can be seen in Fig. 4.

Both w_T and w_H exhibit gradual decay as the centerline is approached, due to the increasing tangential strain-rate, as can be seen in Figs. 4 and 5. Results indicate a general slow-down in the reaction process at the centerline, with notable minima of w_O, w_{OH}, w_{CO}, w_{H_2}, and w_{CH_4}, and of rates of Rxns 1,2.

The above large values of strain-rate are expected to extinguish this flame based on 1D steady-state data[1,2] for stoichiometric methane-air ($K_{ex} = 1650\text{s}^{-1}$). While extinction may occur at later time, it is not observed in the time span of the present results because of the transient nature of the flow. Notably, recent experimental data[17] on flame interaction with a vortex ring suggests that a transient 2D propane flame seems to survive strain-rates that are multiples of its steady-state 1D extinction strain-rate.

Analysis of normal slices of the flame zone at the centerline reveals the influence of unsteady strain-rate on the flame structure. This data demonstrates that one result of large unsteady positive tangential strain-rate is to steepen the profiles of T, Y_{O_2}, and Y_{CH_4}. While these effects may be absent in 1D steady-state strained flames[1], their significance here is related to the transience of the strain-rate field. To consider this matter further, let $\alpha_c = \delta_f^2 \tau_t$ be a "strain-diffusivity" that describes the convective strain effect on the flame structure. Given a value of $\tau_t \approx 14 \times 10^3\text{s}^{-1}$ in the flame, the corresponding diffusivity is found to be $\alpha_c = 17\text{cm}^2/\text{s}$, whereas the thermal diffusivity is $\alpha(T) \approx 3.5\text{cm}^2/\text{s}$. It follows that the temperature profile in the flame is far from a "steady-state", it is being modified by the flow faster than it can relax by diffusion, with $\alpha_c/\alpha \approx 4.9$. Moreover, species concentration fields diffuse with varying mass diffusivities, $D_i(T)$. In particular, the Lewis numbers ($Le_i = \alpha/D_i$) corresponding to the various species span a wide range from $Le_H \approx 0.16$ to $Le_{CO_2} \approx 1.2$, resulting in $\alpha_c/D_H \approx 0.78$, and $\alpha_c/D_{CO_2} \approx 5.9$. Given such diffusional disparities, it is expected that, as different components of the reaction zone respond to unsteady flow disturbances with different time scales, the flame structure is modified accordingly.

The change in flame structure and the resulting drop in reaction rate due to unsteady strain-rate is illustrated in Fig. 6 using the mole fraction profiles of O_2 and H, the temperature, and the rate of progress of Rxn. 1. The profiles are selected at two time instants in a period of increasing tangential strain-rate at the centerline. The steepening of the O_2 and T profiles with time is evident, along with the drop in the rate of Rxn. 1, and the mole

fraction profile of H. There is no observable steepening of the H profile, because of the high diffusivity of H, as indicated above. In particular, note the drop in O_2 mole fraction, due to profile steepening, in the zone where Rxn. 1 is significant. This, along with the drop in H, leads to a slower rate for this reaction, despite the increased temperature in this region, again due to steepening. This reaction is an important chain-branching step in the flame chemistry[2], and its drop is representative of the general slow-down in flame burning rate. Other significant reactions in this region of the flame, such as Rxns. 2-4 and 9, exhibit similar slow-down, leading to a drop in the net rates of production/consumption of H, O, H_2, OH, and CO. The drop in H mole fraction is also symptomatic of that observed with other radicals, such as O and OH, as well as H_2. The lower availability of these species leads to slower rates of hydrocarbon breakdown on the reactants side of the flame. Thus rates of Rxns. 11-17 are observed to drop, along with the net rate of consumption of CH_4 and O_2, and the rates of production of CO_2 and H_2O. This overall slowdown leads to a similar drop in w_T and the net burning rate. Thus, the flame is driven towards extinction by the modification of flame structure due to the unsteady nature of the strain-rate field, and the effect this has on the active radical concentrations crucial to the hydrocarbon breakdown process.

Conclusions

We have studied the detailed unsteady interaction of a flame with a 2D vortex-pair, with regard to the effects of curvature and unsteady strain-rate on flame structure and dynamics. We observe significant flame contortion, consistent with the low Damköhler number of the flow.

We find that the fluxes of intermediate species between the oxidation and fuel consumption layers are affected significantly by flame curvature. Zones of high and low H production and consumption rates are observed at high curvature, consistent with focusing and defocusing arguments related to flame topology, with a net stabilizing result of low burning rate at the curved cusp, convex towards the reactants. While the fluxes of reactants and temperature are also affected by curvature, it is expected that H, which is the fastest diffuser, is a key species in the slow-down of the burning rate in this zone of transient curvature.

High and increasing tangential strain-rate is observed at the flame location along the vortex-pair centerline. Overall slow-down of the reaction process is observed in this zone as the vortex-pair approaches the flame. The transient nature of the flow leads to temporarily high strain-rates at the flame, in excess of the 1D steady extinction strain-rate.

Analysis of the time-development of the profiles of temperature, mole fractions, and reaction rates along the centerline suggest that the unsteady tangential strain-rate leads to steeper profiles of slow-diffusing species and temperature, with less steepening of fast-diffusing species. This modification of flame structure was found to lead to changes in various reaction rates. In particular, the chain-branching reaction $H+O_2 \Longleftrightarrow O+OH$ was observed to proceed at a slower rate due to these stretch-induced changes in flame structure. Other significant reactions in the oxidation layer were similarly affected, leading to lower production rates of active radicals such as H, O and OH, a lower consumption rate of CH_4, and a reduction in the local heat production rate. Larger fractional change was generally observed in the radical chain-branching and recombination reactions on the products side of the flame, versus the hydrocarbon breakdown reactions on the reactants side. While a sensitivity analysis was not presented, these results are consistent with the high sensitivity of the flame to the above chain-branching reaction near extinction, as reported in [2].

While the burning rate at the centerline is observed to decrease in time, the time span of

the present results was not sufficient to observe extinction. This is a matter for future work. Moreover, the quantification of the extinction strain-rate requires a study of the role of the chemical mechanism model[3]. The study of this flow using more realistic C_1-C_2 chemistry is presently underway.

Nomenclature

A_k	pre-exponential factor in Arrhenius expression for $\mathcal{K}_k$
b_k	exponent in Arrhenius expression for $\mathcal{K}_k$
c_p	mixture specific heat at constant pressure
$c_{p,i}$	specific heat at constant pressure, for species i
Da	Damköhler number
D_{iN}	binary mass diffusion coefficient of species i into species N
E_k	activation energy in Arrhenius expression for $\mathcal{K}_k$
K	total flame tangential stretch rate
$\mathcal{K}_k$	elementary reaction rate
M	number of reactions
N	number of species
Pr	Prandtl number
p	dynamic pressure
p_o	stagnation pressure
R	universal gas constant
Re	Reynolds number
Rxn. k	reaction k
Sc	Schmidt number
S_d	flame displacement speed
S_d^u	flame displacement speed referred to the unburnt gas density.
S_L	laminar flame speed
T	temperature
t	time
t_f	flame time scale
t_v	flow time scale
U_θ	typical circumferential flow velocity
$\mathbf{V}_i$	diffusion velocity of species i into the mixture
$\mathbf{v}$	velocity vector, $\mathbf{v} = (u, v)$
$\overline{W}$	local effective molar mass of the mixture

W_i	molar mass of species i
w_i	chemical production rate for species i
w_T	chemical heat source term in energy equation
Y_i	mass fraction of species i

Greek Symbols:

α	thermal diffusivity of gas mixture
δ_f	flame thickness
δ_v	vortex-pair length scale
Φ_x, Φ_y	viscous dissipation terms in Navier-Stokes equations
κ	flame curvature
λ	mixture thermal conductivity
τ_t	tangential strain-rate
μ	dynamic viscosity
ρ	density

Appendix

For present purposes, the flame location is identified by a specified constant level surface of the CH_4 mass fraction. This is set at $Y_{CH_4} = 0.1 Y_{CH_4,max}$. The flame normal, $\mathbf{n}$, and tangential, $\mathbf{t}$, unit vectors are determined relative to the local gradient direction of the Y_{CH_4} surface. Thus, $\mathbf{n} = \nabla Y_{CH_4}/|\nabla Y_{CH_4}|$ points towards the reactants, and $\mathbf{t} \cdot \mathbf{n} = 0$. The tangential strain-rate is evaluated from the strain-rate tensor $\underline{\mathbf{e}}$[12]: $\dot{\epsilon}_t = \mathbf{t} \cdot \underline{\mathbf{e}} \cdot \mathbf{t}$, and the normal strain-rate is $\mathbf{n} \cdot \underline{\mathbf{e}} \cdot \mathbf{n}$. The curvature[19] is defined positive when the flame is convex to the reactants, in 2D: $\kappa = 1/\mathcal{R} = \nabla \cdot \mathbf{n}$, where $\mathcal{R}$ is the radius of curvature.

The flame "displacement" speed[20] is the speed at which the flame "surface" moves relative to the local flow velocity. Thus, with the flame at a constant $Y_{CH_4} = Y_f$, the displacement speed, is defined by:

$$S_d = \left. \frac{-\left(\dfrac{\partial Y_{CH_4}}{\partial t} + \mathbf{v} \cdot \nabla Y_{CH_4} \right)}{|\nabla Y_{CH_4}|} \right|_{Y_{CH_4} = Y_f}.$$

The displacement speed referred to the reactants density is $S_d^u = \rho_f S_d / \rho_u$, where $\rho_f = \rho|_{Y_{CH_4} = Y_f}$. The flame "thickness" is determined from the peak temperature gradient in the flame, and the burnt and unburnt gas temperutures, by $\delta_f = (T_b - T_u)/|\partial T/\partial n|_{max}$.

Acknowledgments

This work was supported by the US Department of Energy, Office of Basic Energy Sciences, Chemical Sciences Division. Discussions with I. Gran and P. Paul contributed greatly to the understanding of the flame-flow interaction.

References

[1] Law, C., *Twenty-Second Symposium (International) on Combustion*, The Combustion Institute, 1988, pp. 1381–1402.

[2] Kee, R., Miller, J., Evans, G., and Dixon-Lewis, G., *Twenty-Second Symposium (International) on Combustion*, The Combustion Institute, 1988, pp. 1479–1494.

[3] Rogg, B., *Combustion and Flame*, 73:45–46 (1988).

[4] Poinsot, T., Veynante, D., and Candel, S., *J. Fluid Mechanics*, 228:561–606 (1991).

[5] Rutland, C., Ferziger, J., and Cantwell, B., Report TF-44, Thermosciences Div., Mech. Eng., Stanford Univ., Stanford, CA, (1989).

[6] Najm, H., *Transport Phenomena in Combustion*, Taylor and Francis, Wash. DC, 1995 in print.

[7] Echekki, T., and Chen, J., *Combustion and Flame* (1996) submitted.

[8] Hilka, M., Veynante, D., Baum, M., and Poinsot, T., *Tenth Symp. on Turbulent Shear Flows*, volume 2, University Park, PA, (1995), Penn. State Univ., pp. 19/19–24.

[9] Baum, M., Poinsot, T., Haworth, D., and Darabiha, N., *J. Fluid Mechanics*, 281:1–32 (1994).

[10] Schlichting, H., *Boundary-Layer Theory,* McGraw-Hill, New York, 7^{th} edition, 1979.

[11] Majda, A., and Sethian, J., *Combustion Science and Technology*, 42:185–205 (1985).

[12] Williams, F., *Combustion Theory,* Addison-Wesley, New York, 2nd edition, 1985.

[13] Smooke, M., and Giovangigli, V., *Reduced kinetic mechanisms and asymptotic approximations for methane-air flames,* , volume 384 of *Lecture Notes in Physics* chapter 1 Springer-Verlag, Berlin, 1991.

[14] GRImech1.2, Gas Research Institute, http://www.gri.org, (1995).

[15] Kee, R., Rupley, F., and Miller, J., Sandia Report SAND89-8009B, Sandia National Labs., Livermore, CA., (1993).

[16] Kee, R., Grcar, J., Smooke, M., and Miller, J., Sandia Report SAND85-8240, Sandia National Labs., Livermore, CA., (1993).

[17] Mueller, C., Driscoll, J., Reuss, D., Drake, M., and Rosalik, M., *Combustion and Flame* (1996) submitted.

[18] Peters, N., in *Turbulent Reactive Flows* (R. Borghi and S. Murthy, Eds.), Springer-Verlag, New York, 1989, pp. 242–256, .

[19] Candel, S., and Poinsot, T., *Combustion Science and Technology*, 70:1–15 (1990).

[20] Poinsot, T., Echekki, T., and Mungal, M., *Combustion Science and Technology*, 81:45–73 (1991).

Figure Captions

Figure 1. Comparison between present scheme and the GRImech-v1.2, for a 1D stoichiometric methane-air flame at atmospheric pressure.

Figure 2. The flow field, after flame contortion by the vortex pair, shown using vorticity and temperature contours. Solid/dashed vorticity contours denote positive/negative vorticity. Positive vorticity is counter-clockwise. The vortex-pair is in the reactants.

Figure 3. Tangential strain-rate and curvature plotted versus a flame length coordinate for the flame in Fig. 2, along half the flame length, from the flame intersection with the edge of the domain to the centerline.

Figure 4. Contours of the heat source term, w_T, illustrating the local reduction in burning rate both at the cusp and at the centerline.

Figure 5. Contours of the production rate of H, w_{H}, showing the variation in production and consumption rates along the flame.

Figure 6. Profiles of O_2 and H mole fractions, Temperature, and rate of progress of reaction 1, scaled by factors of 4, 100, 0.0005, and 70 respectively. Two profiles are plotted for each quantity, with arrows indicating the direction of increasing time and tangential strain rate. The profiles are from normal slices along the vertical centerline, which are superposed to match a reference level of $Y_{\mathrm{CH_4}}$.

Table 1. C_1 skeletal methane-air chemical mechanism. A units are in mole-cm-sec-K, E units are cal/mole.

	Reactions			A	b	E
1.	$H+O_2$	$\Longleftrightarrow$	$O+OH$	8.30e+13	0.0	14413.0
2.	$O+H_2$	$\Longleftrightarrow$	$H+OH$	5.00e+04	2.7	6290.0
3.	$OH+H_2$	$\Longleftrightarrow$	$H+H_2O$	2.16e+08	1.5	3430.0
4.	$2OH$	$\Longleftrightarrow$	$O+H_2O$	3.57e+04	2.4	-2110.0
5.	$H+O_2+M$	$\Longleftrightarrow$	HO_2+M	2.80e+18	-0.9	0.0
	$(O_2{:}0.0, H_2O{:}0.0, CO{:}0.75, CO_2{:}1.5, N_2{:}0.0)$					
6.	$H+HO_2$	$\Longleftrightarrow$	$2OH$	1.34e+14	0.0	635.0
7.	$H+HO_2$	$\Longleftrightarrow$	O_2+H_2	2.80e+13	0.0	1068.0
8.	$OH+HO_2$	$\Longleftrightarrow$	O_2+H_2O	2.90e+13	0.0	-500.0
9.	$OH+CO$	$\Longleftrightarrow$	$H+CO_2$	4.76e+07	1.2	70.0
10.	$H+CH_3(+M)$	$\Longleftrightarrow$	$CH_4(+M)$	1.27e+16	-0.6	383.0
	Low pressure limit: 0.24770e+34 -0.47600e+01 0.24400e+04					
	TROE centering: 0.78300e+00 0.74000e+02 0.29410e+04 0.69640e+04					
11.	$H+CH_4$	$\Longleftrightarrow$	CH_3+H_2	6.60e+08	1.6	10840.0
12.	$OH+CH_4$	$\Longleftrightarrow$	CH_3+H_2O	1.00e+08	1.6	3120.0
13.	$O+CH_3$	$\Longleftrightarrow$	$H+CH_2O$	8.43e+13	0.0	0.0
14.	$H+CH_2O$	$\Longleftrightarrow$	$HCO+H_2$	2.30e+10	1.1	3275.0
15.	$OH+CH_2O$	$\Longleftrightarrow$	$HCO+H_2O$	3.43e+09	1.2	-447.0
16.	$H+HCO$	$\Longleftrightarrow$	H_2+CO	7.34e+13	0.0	0.0
17.	$HCO+M$	$\Longleftrightarrow$	$H+CO+M$	1.87e+17	-1.0	17000.0
18.	CH_3+O_2	$\Longleftrightarrow$	$O+CH_3O$	2.68e+13	0.0	28800.0
19.	$H+CH_3O$	$\Longleftrightarrow$	H_2+CH_2O	2.00e+13	0.0	0.0
20.	$H+CH_2O(+M)$	$\Longleftrightarrow$	$CH_3O(+M)$	5.40e+11	0.5	2600.0
	Low pressure limit: 0.22000e+31 -0.48000e+01 0.55600e+04					
	TROE centering: 0.75800e+00 0.94000e+02 0.15550e+04 0.42000e+04					
21.	$2HO_2$	$\Longleftrightarrow$	$O_2+H_2O_2$	1.30e+11	0.0	-1630.0
22.	$2HO_2$	$\Longleftrightarrow$	$O_2+H_2O_2$	4.20e+14	0.0	12000.0
23.	$2OH(+M)$	$\Longleftrightarrow$	$H_2O_2(+M)$	7.40e+13	-0.4	0.0
	Low pressure limit: 0.23000e+19 -0.90000e+00 -0.17000e+04					
	TROE centering: 0.73460e+00 0.94000e+02 0.17560e+04 0.51820e+04					
24.	$OH+H_2O_2$	$\Longleftrightarrow$	HO_2+H_2O	1.75e+12	0.0	320.0
25.	$OH+H_2O_2$	$\Longleftrightarrow$	HO_2+H_2O	5.80e+14	0.0	9560.0
26.	$H+OH+M$	$\Longleftrightarrow$	H_2O+M	2.20e+22	-2.0	0.0
	$(H_2{:}0.73, H_2O{:}3.65, CH_4{:}2.0)$					
27.	$2H+M$	$\Longleftrightarrow$	H_2+M	1.00e+18	-1.0	0.0
	$(H_2{:}0.0, H_2O{:}0.0, CH_4{:}2.0, CO_2{:}0.0)$					

Table 1. C_1 skeletal methane-air chemical mechanism. A units are in mole-cm-sec-K, E units are cal/mole.

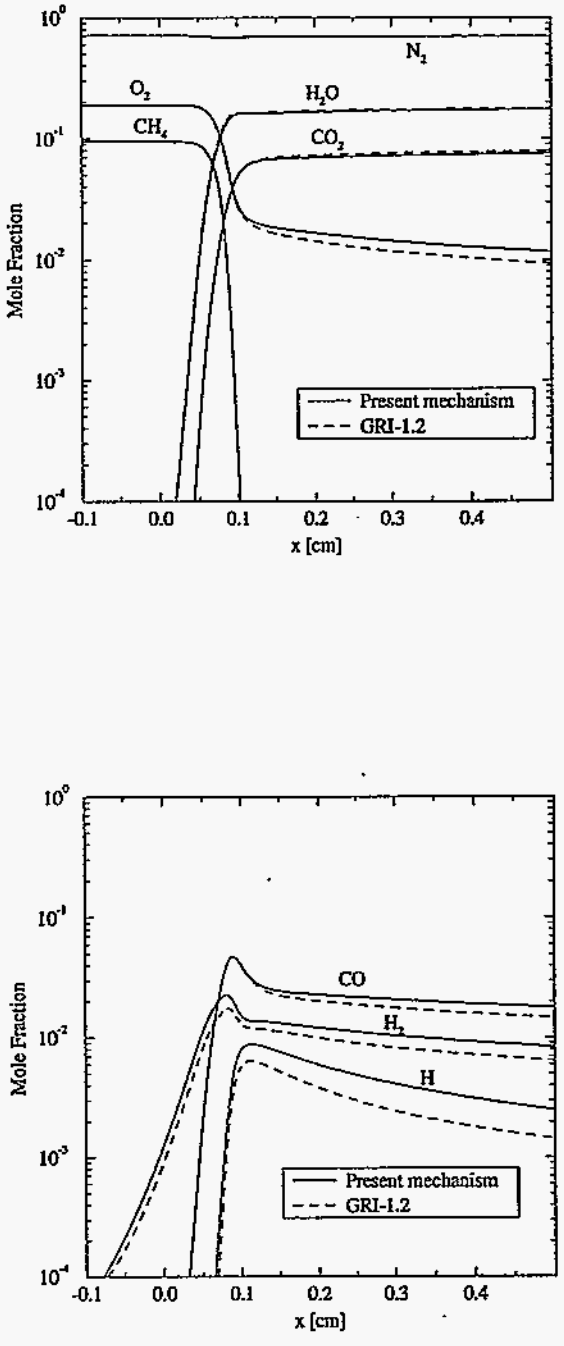

Figure 1. Comparison between present scheme and the GRImech-v1.2, for a 1D stoichiometric methane-air flame at atmospheric pressure.

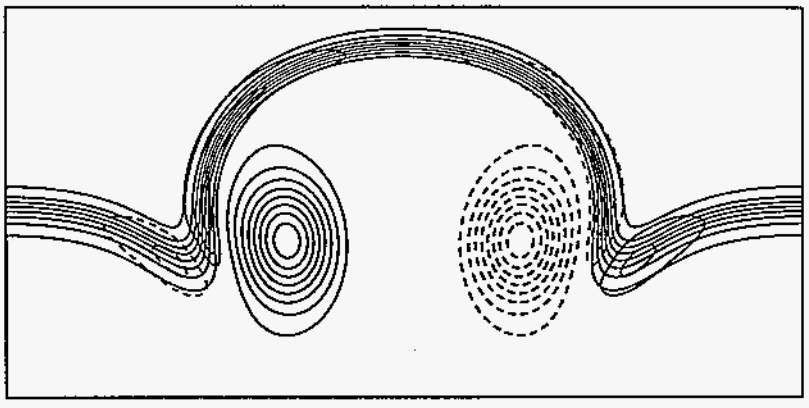

Figure 2. The flow field, after flame contortion by the vortex pair, shown using vorticity and temperature contours. Solid/dashed vorticity contours denote positive/negative vorticity. Positive vorticity is counter-clockwise. The vortex-pair is in the reactants.

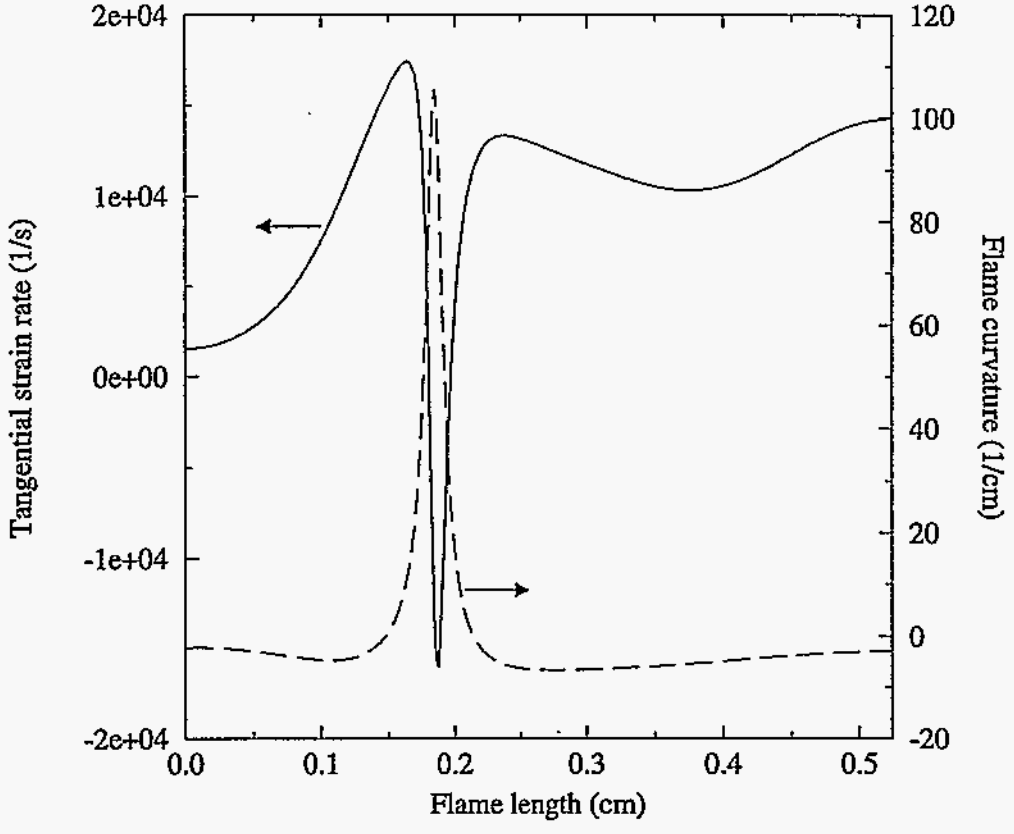

Figure 3. Tangential strain-rate and curvature plotted versus a flame length coordinate for the flame in Fig. 2, along half the flame length, from the flame intersection with the edge of the domain to the centerline.

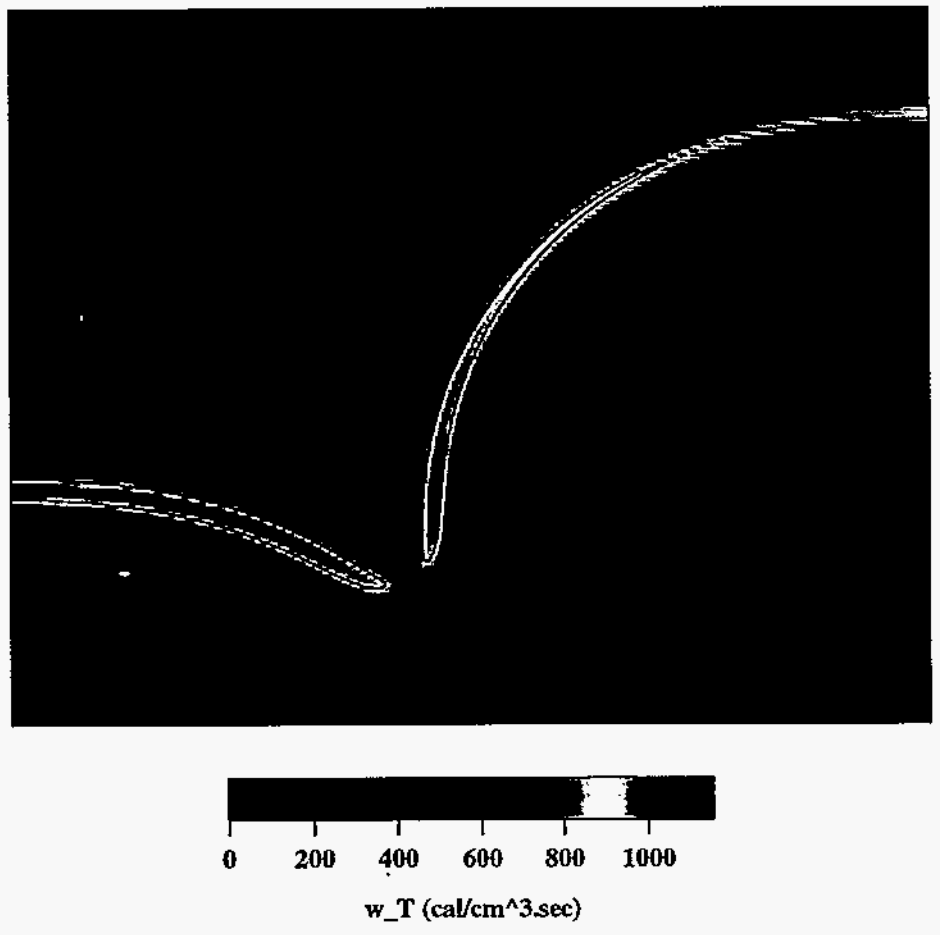

Figure 4. Contours of the heat source term, w_T, illustrating the local reduction in burning rate both at the cusp and at the centerline.

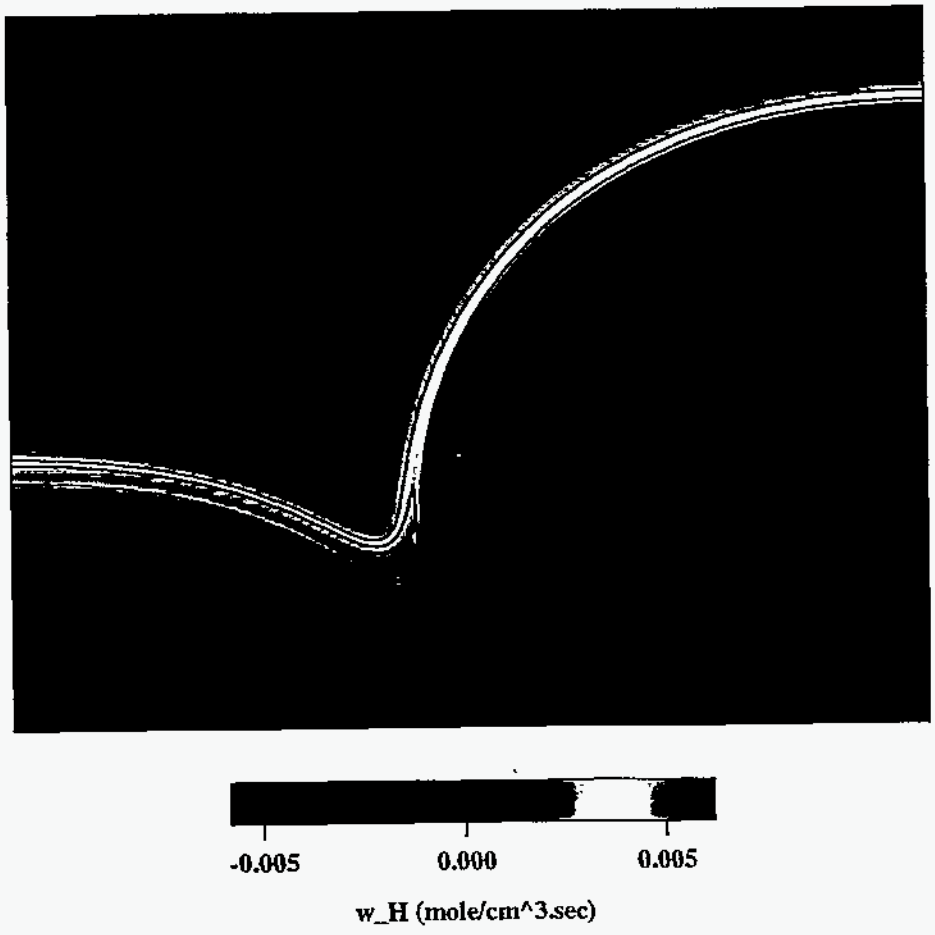

Figure 5. Contours of the production rate of H, w_H, showing the variation in production and consumption rates along the flame.